Department of the Navy
Office of Naval Research
Contract N6onr-244 - Task II

THE DESIGN OF AXIAL FLOW PUMPS

R. D. Bowerman

Hydrodynamics Laboratory
California Institute of Technology
Pasadena, California

Report No. E-19.10

April 1956

(Reprinted from the Transactions of the ASME for November, 1956, with permission of Copyright Owner)

The Design of Axial Flow Pumps[1]

By R. D. BOWERMAN,[2] PASADENA, CALIF.

A design procedure for axial-flow pump impellers is presented that accounts for induced interference effects in the prediction of performance. Induced interference velocities at an impeller blade have been calculated using a three-dimensional model that includes the effects of the other blades and of the total downstream vorticity along the center line of the pump. The design method considers improvement of cavitation conditions by specifying the radial variation of the design parameters such that the pressure distributions on all radial sections are similar. An analysis of optimizing the impeller geometric parameters for cavitation conditions is presented to permit the initial choices of the quantities appearing in the design procedure. Experimental work on a two-bladed impeller has yielded results that give good support to all aspects of the design method.

Nomenclature

The following nomenclature is used in the paper:

a = annular area of impeller = $\pi(r_2^2 - r_1^2)$
A, B = constants appearing in streamline equation
C_θ = dimensionless tangential interference velocity = $\frac{V_\theta r_2}{\Gamma_b}$, given by the linearized equation

$$C_\theta = K_0 + K_1(\xi/\xi_t)$$

C_p = static head coefficient = $\frac{(h_s - H_T)g}{u_2^2}$
ΔC_p = static head differential coefficient
C_L = lift coefficient
C_{l_i} = design section lift coefficient
c = chord
g = gravitational constant
H = head of impeller
H_0 = free-stream total pressure, psi (as in reference 9)
H_T = total head in impeller eye
h_s = local static head
K_0, K_1 = constants in equation for C_θ
L' = lift force per unit width
N = rpm
n = number of blades
P = local static pressure
P_t = total pressure in impeller eye
P_v = vapor pressure
Q = flow rate, cfs
q_0 = free-stream dynamic pressure
R = reaction
r = radial co-ordinate
S = blade pressure-distribution coefficient
s = spacing = $2\pi r/n$
T = torque
u = impeller speed = ωr
V = velocity
V_R = relative velocity (average)
V_θ = tangential component of interference velocity
V_a = axial velocity (through-flow)
x = co-ordinate along chord line
y = co-ordinate perpendicular to chord line
z = axial co-ordinate
β = angle from horizontal
β_c = blade angle (chord-line angle)
Γ_b = circulation of a single blade
Γ = total circulation value
η = radius ratio = r/r_2
η_1 = hub ratio = 0.6 for this work
η^* = efficiency
θ = angular co-ordinate, also camber angle
ξ = dimensionless axial co-ordinate
ξ_t = axial extent ratio = z_t/r_2
ρ = fluid density
σ = cavitation coefficient = $\frac{\text{NPSH}}{H} = -\frac{C_p}{\psi}$
τ = torque coefficient = $\frac{T}{\rho a u_2^2 r_2}$
ϕ = flow-rate coefficient = $V_a/u_2 = Q/au_2$
χ_ω = speed coefficient = $\frac{\omega Q^{1/2}}{\pi^{1/2}(1-\eta_1^2)^{1/2}H^{3/4}g^{3/4}}$
χ_{r_2} = size coefficient = $r_2\frac{H^{1/4}g^{1/4}\pi^{1/2}(1-\eta_1^2)^{1/2}}{Q^{1/2}}$
ψ = head coefficient = $\frac{Hg}{u_2^2}$
ψ' = input head coefficient = τ/ϕ
ω = angular velocity
c/s = solidity
NPSH = net positive suction head
N_s = specific speed = $\frac{NQ^{1/2}}{H^{3/4}}$
N_{ss} = suction specific speed = $\frac{NQ^{1/2}}{(\text{NPSH})^{3/4}}$
$\frac{v}{V}$ = velocity ratio due to thickness
$\frac{\Delta v}{V}$ = velocity ratio due to camber
$\Delta v_a/V$ = velocity ratio due to angle of attack

Subscripts

1 = hub radius; also, angle at leading edge
2 = case radius; also, angle at trailing edge
t = trailing edge
b = refers to a single blade
s = streamline quantity
i = isolated airfoil quantity
∞ = far downstream
e = design-point value

[1] This work was supported by the Office of Naval Research, under Contract N6onr-244, Task Order 2. Reproduction in whole or in part is permitted for any purpose of the U. S. Government.

[2] Research Engineer, Hydrodynamics Laboratory, California Institute of Technology. Assoc. Mem. ASME.

Contributed by the Hydraulic Division and presented at the Diamond Jubilee Annual Meeting, Chicago, Ill., November 13–18, 1955, of The American Society of Mechanical Engineers.

Note: Statements and opinions advanced in papers are to be understood as individual expressions of their authors and not those of the Society. Manuscript received at ASME Headquarters, August 25, 1955. Paper No. 55—A-127.

Introduction

In recent years, axial-flow pump impellers have been designed by applying the data of two-dimensional isolated airfoil theory to each cylindrical section of a blade. In general, the results have been good. However, there has been some disagreement and doubt as to the corrections that should be applied to the two-dimensional airfoil sections when they are subjected to the influence of the cylindrical boundaries of the pump where there are mutual interference effects between the blades. Previous attempts to account for interference have been based on calculations of simple cascades of airfoils in two dimensions. Following the general suggestions of Spannhake (4),[3] the present design procedure uses corrections based on a three-dimensional model, i.e., with the blades treated as spokes of a wheel.

The design method proposed includes the very important consideration of designing for optimum cavitation conditions. The basic presumption in the cavitation consideration is that the blade-pressure distribution can be closely predicted by the correction process of the design procedure. Optimum cavitation design is meant to describe the choosing of the optimum speed and size in connection with the performance desired to give the impeller the least susceptibility to cavitation. It is thought that making all radial sections equally susceptible to cavitation produces a pump with better over-all cavitation performance. The optimizing analysis affords the first step in the design procedure by permitting proper choices of the blade-section coefficients, the number of blades and the approximate geometric quantities and speed of operation. The interference corrections are then applied to determine the finished blade-section shapes.

It is only proper to concede that the present correction for blade mutual interference method of designing is based on assumptions that are not entirely proved. Furthermore, theories that may be employed in the design of turbomachinery are still subject to argumentation. Cascade theories are reasonably accurate in the design of axial-flow compressors; however, it is shown in the present work that cascade theories do not give proper predictions of pump-impeller operation. The present three-dimensional interference calculation and two-dimensional cascade calculations do not agree. Also, there apparently is no logical transition between the two-dimensional flow model and the three-dimensional model which will allow a continuous theory for turbomachine design. The author suggests continuation of investigations of turbomachine theories; however, this presentation is made in the belief that it now offers worthwhile improvements over existing axial-flow-pump design methods.

An extensive experimental study of a two-bladed impeller designed by the three-dimensional method has been conducted and the results are presented. As this impeller represents a nominal specific speed (10,000) of the usual axial-flow designs, it is presumed that the experimental results substantiate the use of the design method for most axial-flow pumps. The limitations on the present method are not known and further experimental verifications are needed—especially in the realm of lower specific speeds where the solidity must become high.

The Interference Calculation

The basis of the design procedure is to fit a camber line to a curving streamline in the annular-blade region in the same manner that a camber line is placed on a straight streamline for an isolated airfoil in an infinite field of uniform flow. The performance of the designated camber line is then assumed to be the same in both cases. The fact that the relative flow is slightly retarded is neglected. The main consideration then is to determine the curved streamline which is composed of the through-flow velocity, the tangential velocity of the impeller, and the induced interference velocities from all sources. Thickness effects have been neglected and only vorticity has been considered. The total vorticity effect cannot easily be handled; therefore the interference has been calculated by approximating the total influence by the influence of the vorticity of the blades from the case to the hub center line and downstream on the center line to infinity. Case and hub boundary conditions were placed in effect. The center-line vorticity of the "removed" blade has been included, but the cyclic effect of the removed blade (if there is such an effect) has been omitted.

The interference of the center-line vorticity of the removed blade was found using the equation derived in a previous work (1) where it was assumed that the vorticity grows linearly through the blade row. The exact solution is

$$C_{\theta b} = \frac{V_{\theta b} r_2}{\Gamma_b} = \frac{1}{4\pi\eta}\left[1 + \frac{1}{\xi_t}\left(\sqrt{\xi^2 + \eta^2} - \sqrt{(\xi_t - \xi)^2 + \eta^2}\right)\right] \quad \ldots\ldots [1]$$

The interference velocity depends on the axial extent of the blade and on the radius ratio. Typical curves of the dimensionless interference velocity of the removed blade are shown in Fig. 1.

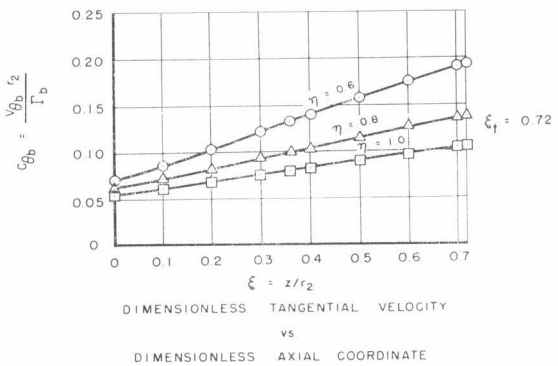

Fig. 1 Induced Tangential Velocity Due to Downstream Vorticity of a Blade for the Example $\xi_t = 0.72$

The interference velocities due to the other blades were found by employing the velocity values due to a single vortex element as presented by H. N. Tyson, Jr. (2). The solution presented by Tyson did not lend itself to rapid calculations and could not be further analytically summed to represent a blade with distributed vorticity. Therefore graphical summations of the limited data Tyson presented were made for several blade representations. It was necessary to add to Tyson's values correction values due to a center-line vorticity of $\Gamma/2$ (per blade) to achieve conditions of zero prewhirl and total circulation downstream as Tyson considered symmetrical splitting of the radial vortex element, half upstream and half downstream. Also, only the tangential component was retained in the final interference analysis, as the radial and axial components are comparatively small. Interference-velocity values were summed for four values of the axial extent ratio $\xi_t = z_t/r_2 = 0.2$, 0.4, 0.6, and 0.72. A single vortex element was used to approximate the blade vorticity for $\xi_t = 0.2$, three vortices of equal strength dispersed along the chord line for $\xi_t = 0.4$, and five vortices for $\xi_t = 0.6$ and 0.72. These very approximate blade representations are believed to be satisfactory for the solidities involved in these summations. In instances where greater values of ξ_t and greater numbers of blades combine to give high solidity, then more precise distribution of the blade

[3] Numbers in parentheses refer to the Bibliography at the end of the paper.

vorticity would be necessary. Dispersion of the singularities could be made only along a single helical surface (corresponding to a blade angle of 32.4 deg at the hub and 20.9 deg at the case). Actual blade angles can be a few degrees different from this helical representation without suffering serious error. Summations were made at the hub, mid-radius, and tip sections. Blade representation and summation regions are illustrated in Fig. 2 for the case $\xi_t = 0.4$.

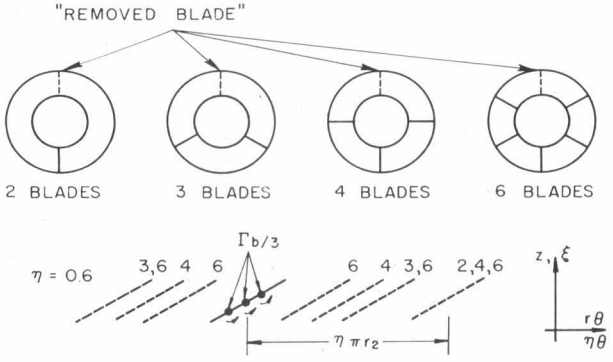

BLADE REPRESENTED BY THREE VORTICES WITH $\xi_t = 0.4$

THE DOTTED LINES SHOW THE SUMMATION REGIONS AND THE NUMBERS ABOVE CORRESPOND TO THE NUMBER OF BLADES ON THE IMPELLER

FIG. 2 TYPICAL BLADE REPRESENTATIONS FOR SUMMATION OF MUTUAL INTERFERENCE VELOCITIES

The final total interference is the sum of the effects of the other blades and the downstream vorticity of the removed blade. In Fig. 3 values of the total tangential interference velocity are plotted against the axial-blade extent ($\xi = z/r_2$) for the case of a two-vaned impeller with $\xi_t = 0.72$. The shape of these curves is typical of all cases summed.

As the curves deviate only slightly from straight lines, each curve for the dimensionless induced tangential velocity (C_θ) was approximated by a line with the equation

$$C_\theta = K_0 + K_1(z/z_t) \quad \ldots\ldots\ldots\ldots\ldots\ldots [2]$$

where K_0 is the interference-velocity value at the removed blade leading edge and K_1 is the difference in values between the trailing edge and leading edge. The value of z/z_t varies from 0 to 1 from the leading edge to trailing edge. In this manner, all of the cases have been reported by presenting values of the constants K_0 and K_1. In Table 1 these values are tabulated and, in Fig. 4(a),

TABLE 1 VALUES OF K_0 AND K_1, DEFINING TOTAL INDUCED TANGENTIAL VELOCITY

Axial extent	No. of blades	K_0			K_1		
		$\eta = 0.6$	$\eta = 0.8$	$\eta = 1.0$	$\eta = 0.6$	$\eta = 0.8$	$\eta = 1.0$
$\xi_t = 0.2$	2	0.212	0.180	0.134	0.106	0.038	0.051
	3	0.299	0.269	0.186	0.198	0.059	0.105
	4	0.371	0.352	0.231	0.319	0.092	0.174
	6	0.463	0.501	0.304	0.665	0.192	0.348
$\xi_t = 0.4$	2	0.180	0.161	0.118	0.170	0.076	0.083
	3	0.241	0.235	0.156	0.315	0.128	0.159
	4	0.274	0.288	0.180	0.514	0.220	0.277
	6	0.289	0.310	0.191	1.015	0.574	0.574
$\xi_t = 0.6$	2	0.152	0.142	0.103	0.227	0.114	0.112
	3	0.183	0.187	0.125	0.430	0.224	0.228
	4	0.187	0.191	0.128	0.687	0.415	0.381
	6	0.191	0.184	0.127	1.210	0.826	0.701
$\xi_t = 0.72$	2	0.135	0.130	0.093	0.258	0.137	0.129
	3	0.149	0.159	0.103	0.493	0.280	0.268
	4	0.138	0.144	0.100	0.781	0.505	0.433

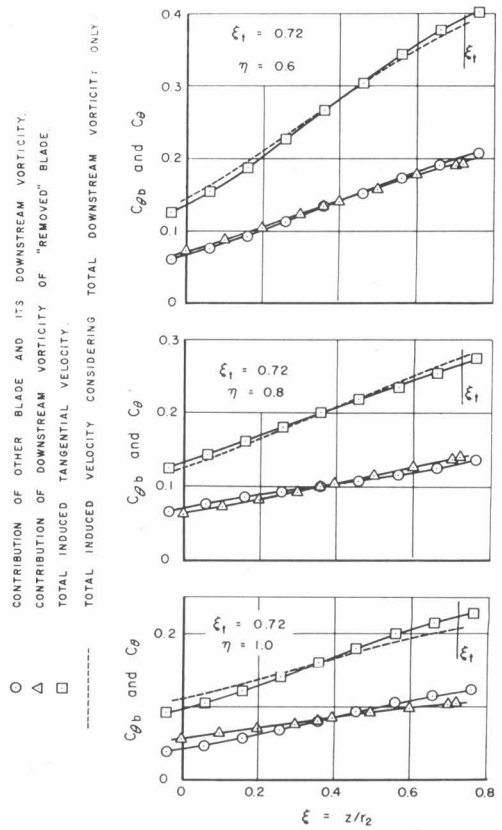

FIG. 3 TANGENTIAL INTERFERENCE VELOCITIES AS A FUNCTION OF THE AXIAL CO-ORDINATE FOR THE EXAMPLE OF A TWO-BLADED IMPELLER WITH $\xi_t = 0.72$

K_0 and K_1 are plotted as functions of the radius ratio. It should be noted that C_θ is the dimensionless total interference velocity equal to $V_\theta r_2/\Gamma_b$ where V_θ is the total interference velocity and Γ_b is the value of circulation of a single blade. Γ_b is used because the number of blades is taken into account in the summation and so included in the values of K_0 and K_1.

It is of interest to note that the present interference calculation supports certain known limits concerning fluid flows. In the three-dimensional calculation there cannot be a limit that corresponds to the isolated airfoil; however, the case of zero blades has a similar significance. In Fig. 4(b) a plot of the K_0 and K_1 values are shown as functions of the number of blades on an impeller. It can be seen that K_0 and K_1 approach zero for zero blades corresponding to no interference effects. The limit as the number of blades is increased is the Euler result for an infinite number of blades. This limit requires exact guidance of the flow, so the total circulation must be achieved at the impeller exit. In other words, the "interference" is the total effect of the impeller. Therefore K_0 must become zero and K_1 become equal to the total circulation velocity. It can be seen (Fig. 4b) that the K_0-curves do seem to reach a maximum and begin to approach zero as the number of blades is increased. Similarly K_1 appears to approach the total tangential circulation velocity. Fig. 4(b) also shows that neither isolated airfoil data alone nor Euler theory can give correct results for designing pump impellers.

The effect of the axial extent of the blades is demonstrated in Figs. 4(a) and 4(b). If the axial extent is small, K_0 is near to half the total circulation far downstream. K_0 becomes smaller as the

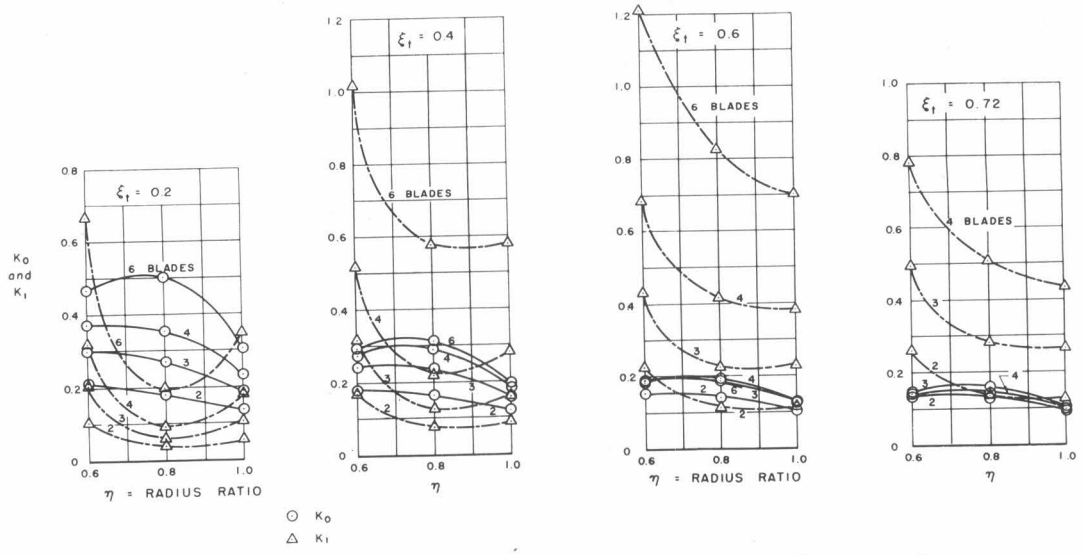

FIG. 4(*a*) K_0 AND K_1 AS FUNCTIONS OF THE RADIUS RATIO FOR SEVERAL NUMBERS OF BLADES

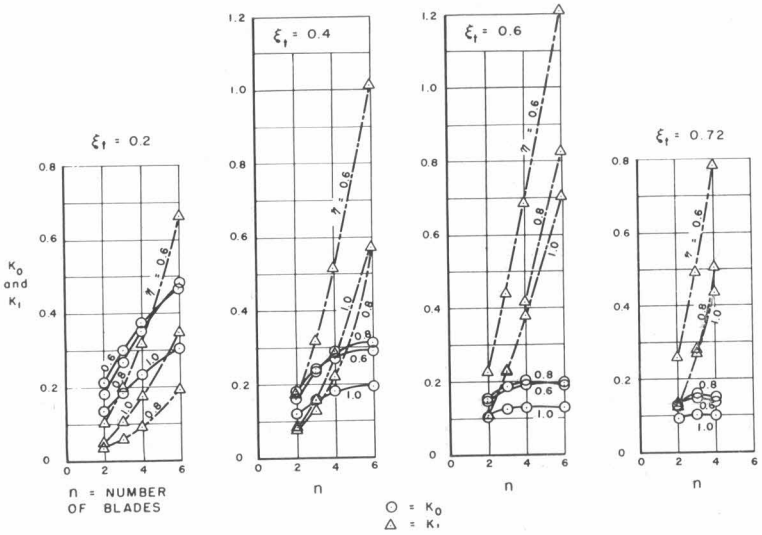

FIG. 4(*b*) K_0 AND K_1 AS A FUNCTION OF THE NUMBER OF BLADES

axial extent increases. On the other hand, as the axial extent gets small K_1 approaches zero and for large axial extent K_1 becomes large. These results show that as the axial extent of the blade becomes large with respect to the case radius of the pump, more of the circulation growth occurs within the blade region.

In Fig. 3 the individual contributions to the total induced velocity have been plotted as well as the total value. It can be seen that the effect of another blade and its downstream vorticity is little different than the downstream effect of the removed blade. The effects of the mutual blade interference are compared to the effects of the total downstream vorticity by the dotted curves which represent simply the downstream vorticity results multiplied by the number of blades on the impeller. For the two-vaned case given in Fig. 3, the separate effect of the other blade is seen to be small. It appears, then, that two-vaned impellers with small axial extent might be designed with reasonable success by considering only the downstream vorticity. However, when the axial extent is large, or there are several blades, then mutual blade interference should be included.

THE DESIGN EQUATIONS

An impeller blade is designed by placing a camber line on the pre-existing streamline in the blade region. The camber line could be put on the streamline at an angle of attack; however, for consideration of improved cavitation conditions it is thought that the best way to achieve the design head is by using camber only rather than by operation at angle of attack. Normally for a cambered blade shape, shockless entry occurs approximately at zero angle of attack to the chord line and a smoother pressure distribution is obtained. If the pressure distribution has a large negative area at the leading edge, which is the case with angle of attack, then cavitation is more likely to occur.

The streamline equation is derived from the geometric relation illustrated in Fig. 5(*a*). It is seen that

$$\tan \beta = \frac{dz}{rd\theta} = \frac{Va}{u - V_\theta} = \frac{Va}{u - \dfrac{\Gamma_b}{r_2} C_\theta}$$

C_θ is given by Equation [2].

Integrating, solving for θ, and introducing the dimensionless parameters ϕ_e, ξ, and η gives

$$\theta = \frac{\xi}{\phi_e} - \frac{\Gamma_b}{\phi_e r_2^2 \omega \eta}\left[K_0 \xi + \frac{K_1 \xi^2}{2\xi_t}\right] \quad \ldots\ldots\ldots [3]$$

The hub blade angle β_{c1} is determined as follows

$$\tan \beta_{c1} = \frac{z_t}{r_1 \theta_{1t}} = \frac{\xi_t}{\eta_1 \theta_{1t}}$$

where θ_{1t} is the value of θ at the trailing edge of the root section. Substituting Equation [3] for θ_{1t} (properly evaluated), then

$$\cot \beta_{c1} = \frac{\eta_1}{\phi_e} - \frac{\Gamma_b}{\phi_e \omega r_2^2}\left[K_{01} + \frac{K_{11}}{2}\right] \quad \ldots\ldots\ldots [4]$$

where K_{01} and K_{11} are the interference velocity constants at the root section.

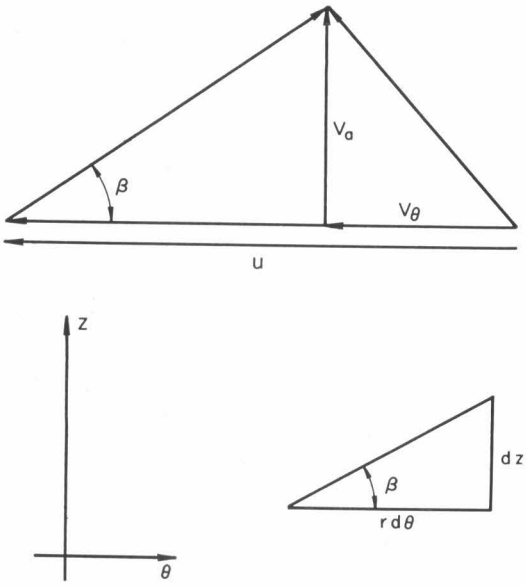

FIG. 5(a) VELOCITY COMPONENTS AND THE CO-ORDINATE SYSTEM

Lift coefficient is introduced from the equations of airfoil theory

$$L' = \rho V \Gamma_b = \frac{1}{2} \rho V^2 c C_L$$

where V is approximated by V_R average—the average relative velocity

$$V \cong V_R \cong \frac{V_a}{\sin \beta_c}$$

Solving for Γ_b, dividing through by ωr_2^2, and evaluating at the root section produces

$$\frac{\Gamma_b}{\omega r_2^2} = \frac{1}{2} \phi_e \xi_t \frac{C_{L1}}{\sin^2 \beta_{c1}} \quad \ldots\ldots [5]$$

Equations [4] and [5] may be resolved for ϕ_e and $\Gamma_b/\omega r_2^2$ with the results

$$\phi_e = \frac{2\eta_1 \sin \beta_{c1}}{2 \sin \beta_{c1} \cos \beta_{c1} + \xi_t C_{L1} \left(K_{01} + \frac{K_{11}}{2} \right)} \quad \ldots\ldots [6]$$

$$\frac{\Gamma_b}{\omega r_2^2} = \frac{\xi_1 \eta_1 C_{L1}}{2 \sin \beta_{c1} \cos \beta_{c1} + \xi_t C_{L1} \left(K_{01} + \frac{K_{11}}{2} \right)} \quad \ldots\ldots [7]$$

and also

$$\frac{\Gamma_b}{\phi_e \omega r_2^2} = \frac{C_{L1} \xi_t}{2 \sin^2 \beta_{c1}} \quad \ldots\ldots [8]$$

Equation [3] can be rewritten as

$$\theta = A\xi - \frac{B}{\eta} \left(K_0 \xi + \frac{K_1 \xi^2}{2 \xi_t} \right) \quad \ldots\ldots [9]$$

where $A = 1/\phi_e$ and ϕ_e is given by Equation [6] and B is given by Equation [8]. A and B are constants determined by the performance desired and depend on the choices of the parameters C_{L1}, ξ_t, ω, and the number of blades n. K_0 and K_1 depend upon the number of blades and the axial extent ratio ξ_t, and are functions of the radius.

The variation of the amount of the camber (lift coefficient) with radius is determined thus: From airfoil theory

$$C_L = \frac{2\Gamma_b}{V_R c}$$

where $V_R = Va/\sin \beta_c$, $c = z_t/\sin \beta_c$, and $Va = \omega r_2 \phi_e$. Combining these expressions with Equation [8] gives

$$C_L = \frac{C_{L1} \sin^2 \beta_c}{\sin^2 \beta_{c1}} \quad \ldots\ldots [10]$$

The blade angle β_c varies with radius as determined from the relation $\tan \beta_c = \xi_t/\eta\theta_t$. Equation [9] gives the value of θ_t. Thus

$$\beta_c = \cot^{-1} \left[A\eta - B \left(K_0 + \frac{K_1}{2} \right) \right] \quad \ldots\ldots [11]$$

The head coefficient is found by considering the theoretical head relation for zero prewhirl

$$H = \frac{u V_{\theta\infty}}{g}$$

Then

$$\psi_e = \frac{Hg}{u_2^2} = \frac{u V_{\theta\infty}}{u_2^2} = \frac{r V_{\theta\infty}}{\omega r_2^2}$$

where all values are taken at the design flow rate. Since

$$V_{\theta\infty} = \frac{n \Gamma_b}{2\pi r}$$

is the circulation velocity far downstream, then

$$\psi_e = \frac{n \Gamma_b}{2\pi \omega r_2^2} \quad \ldots\ldots [12]$$

$\Gamma_b/\omega r_2^2$ is given in Equation [8].

When all of the performance quantities and parameters have been chosen properly by the cavitation-optimizing analysis, the streamline constants A and B can be calculated from Equations [6] and [8] and the streamline co-ordinates can be computed from Equation [9]. The values of the blade angle at various radii are calculated from Equation [11], and the variations of C_L are determined from Equation [10]. These are the necessary quantities to determine the final blade shape.

DESIGNING FOR OPTIMUM CAVITATION CONDITIONS

Investigations of the best relations between size and speed to reduce cavitation susceptibility in pumps have been made in the past. The analyses have usually been made at the tip section of the impeller which was considered to be the critical section for cavitation. If the cavitation due to tip clearance flow is neglected, then it seems reasonable that the over-all cavitation susceptibility might be reduced if the impeller blades were designed with all radial sections equally critical. If the effect of the thickness function on minimum static pressure can be assumed to vary only slightly with change in radius, then the pressure distribution at each radius can be made equal by considering the head produced at each radial section. For a free-vortex design, the head is constant for all radial sections. It can be shown that to achieve the same head at each section, the tangential force must be the same; so to have similar pressure distributions (same minimum pres-

sures) the axial extent of a blade must be the same at all radii. In this manner the chord increases from hub to case as the cosecant of the chord angle in contrast to past designs where the chord was kept nearly constant. By the foregoing qualitative reasoning, constant axial extent is specified in the design procedure.

With each radial section equally susceptible to cavitation, the hub section will be given preference in the optimizing procedure since it will have the highest loading. Combining the method of calculating approximate pressure distributions on isolated airfoils as given in reference (9) with the geometric relations concerning the flow through a pump, permits calculating the incipient cavitation coefficient σ = NPSH/H as a function of specific speed and of the impeller size. (Note σ here stands for incipient cavitation and not cavitation breakdown.) The equation for the pressure distribution is

$$S = \frac{H_0 - P}{q_0} = \left[\frac{v}{V} + \frac{C_L}{C_{Li}}\frac{\Delta v}{V} + \frac{\Delta v_a}{V}\right]^2 \quad \ldots\ldots [13]$$

where

$$H_0 = \frac{1}{2}\rho V_R^2 + P_T - \frac{1}{2}\rho V_a^2$$

$$q_0 = \frac{1}{2}\rho V_R^2$$

and

$$V_a = V_R \sin\beta_c \text{ (as seen in Fig. 5}b\text{)}$$

The term $\Delta v_a/V$ is the pressure drop due to angle of attack which is neglected by virtue of specifying that the optimum operation is at zero angle of attack. When $P = P_v$, the vapor pressure of the liquid, then cavitation is imminent. Equation [13] can be rearranged giving

$$\text{NPSH} = \frac{P_t - P_v}{\rho g} = \frac{V_R^2}{2g}(S - 1 + \sin^2\beta_c)$$

$$= \frac{V_a^2}{2g}\left(\frac{S-1}{\sin^2\beta_c} + 1\right) \quad \ldots\ldots [14]$$

From the head relations

$$\psi_e = \frac{H_e g}{u_2^2} \text{ and } H_e = \frac{uV_{\theta\infty}}{g}$$

then

$$V_{\theta\infty} = \frac{\psi_e u_2}{\eta}$$

Also, with $\phi_e = V_a/u_2$, and employing the velocity triangle (Fig. 5b) the chord angle is determined

$$\beta_c = \cot^{-1}\left(\frac{\eta - \frac{\psi_e}{2\eta}}{\phi_e}\right) \quad \ldots\ldots [15]$$

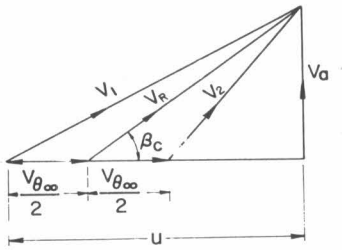

FIG. 5(b) INLET, OUTLET, AND MEAN VELOCITY TRIANGLE

Dividing through Equation [14] by the head gives

$$\sigma = \frac{\text{NPSH}}{H} = \frac{\phi_e^2}{2\psi_e}\left(\frac{S-1}{\sin^2\beta_c} + 1\right) \quad \ldots\ldots [16]$$

Two dimensionless quantities may be defined from ϕ_e and ψ_e, one dependent only on speed and the other on size

$$\chi_\omega = \frac{\phi_e^{1/2}}{\psi_e^{3/4}} = \omega\frac{Q^{1/2}}{\pi^{1/2}(1-\eta_1^2)^{1/2}H^{3/4}g^{3/4}} \quad \ldots\ldots [17]$$

$$\chi_{r_2} = \frac{\psi_e^{1/4}}{\phi_e^{1/2}} = r_2\frac{H^{1/4}g^{1/4}\pi^{1/2}(1-\eta_1^2)^{1/2}}{Q^{1/2}} \quad \ldots\ldots [18]$$

Then Equation [16] can be rewritten as

$$\sigma = \chi_\omega\chi_{r_2}\frac{\phi_e^2}{2\psi_e^{1/2}}\left(\frac{S-1}{\sin^2\beta_c} + 1\right) \quad \ldots\ldots [19]$$

The specific speed for a hub ratio η_1 of 0.6 is

$$N_s\left(\frac{\text{rpm (gpm)}^{1/2}}{\text{ft}^{3/4}}\right) = 3880\chi_\omega \quad \ldots\ldots [20]$$

In Fig. 6, σ is plotted as a function of N_s for various values of

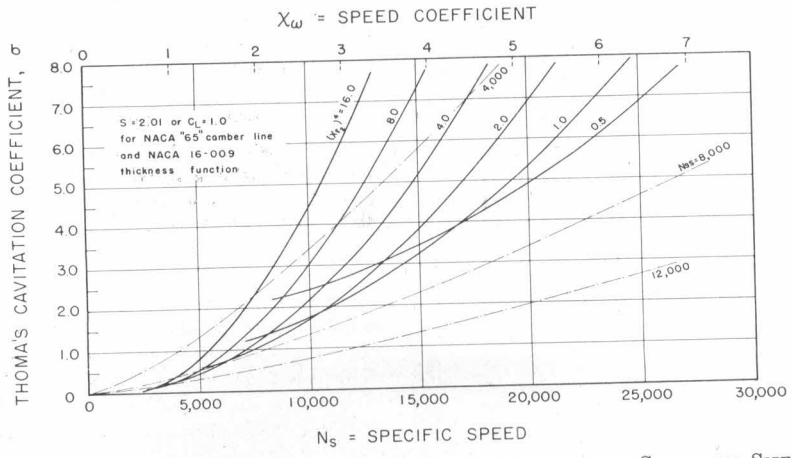

FIG. 6 EXAMPLE OF CAVITATION COEFFICIENT AS A FUNCTION OF SPEED AND SIZE FOR A PARTICULAR BLADE SECTION
(NACA 65 refers to the camber type found in reference 9.)

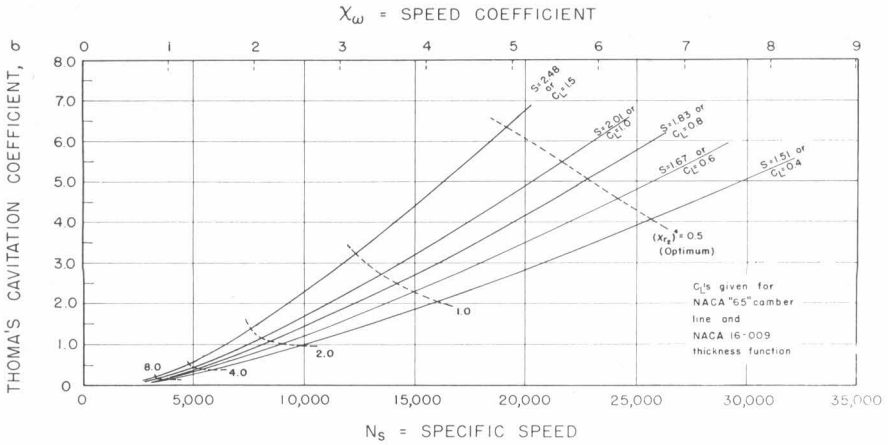

FIG. 7 OPTIMUM σ FOR SEVERAL VALUES OF S OR C_L

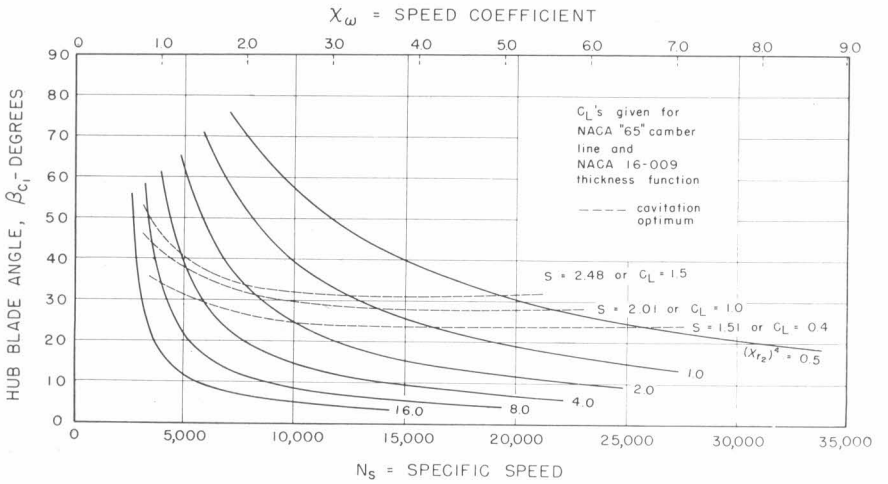

FIG. 8 HUB BLADE ANGLE AS A FUNCTION OF SPEED AND SIZE

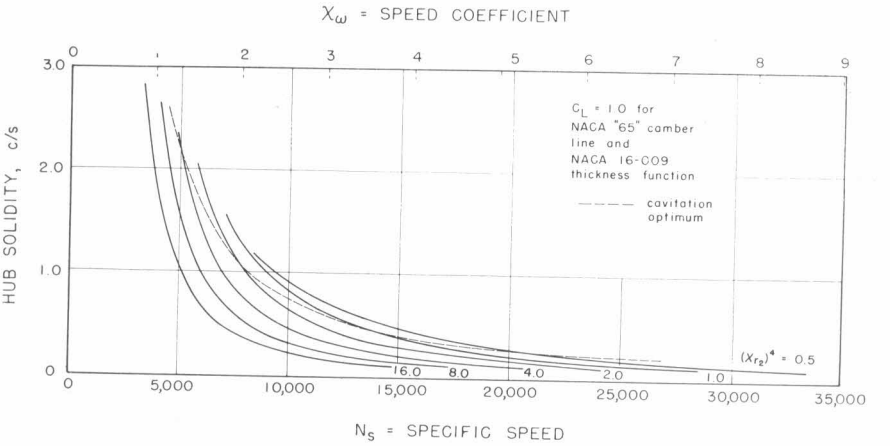

FIG. 9 SOLIDITY (c/s) AS A FUNCTION OF SPEED AND SIZE FOR ONE PARTICULAR BLADE SHAPE

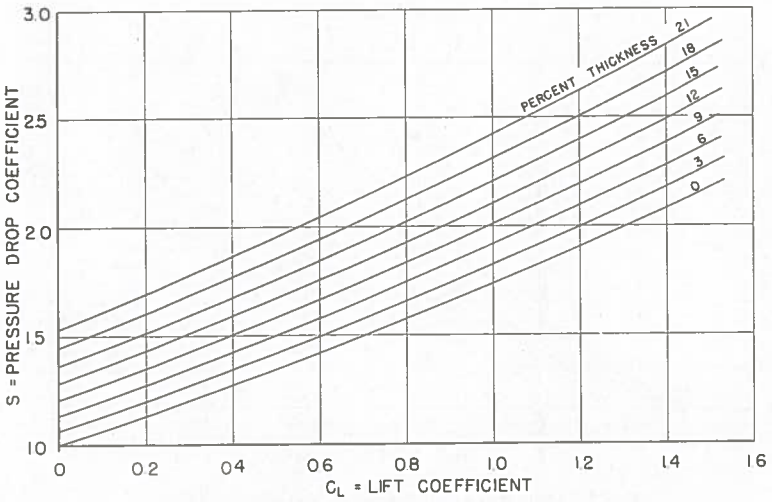

FIG. 10 PRESSURE-DROP COEFFICIENT S AS A FUNCTION OF C_L AND PER CENT THICKNESS FOR SYMMETRICAL PARABOLIC CAMBER LINES (NACA 65 and NACA series 16 thickness functions.)

$(\chi_{r_2})^4$ for a particular blade-section shape. In this example a value of $S = 2.01$ resulted from a symmetrical parabolic camber and an NACA 16-009 thickness function.[4] It can be seen that for a given specific speed, there is a particular impeller size that will provide the best (lowest) cavitation coefficient σ. The envelope of these curves represents the best cavitation conditions possible for the given blade section. Fig. 7 shows the enveloped curves for several values of S or C_L. With curves such as shown in Figs. 6 and 7, for a given Q and H, either N or σ may be specified and the resultant optimum size and blade section coefficient can be determined. Other resultant quantities have been calculated; the hub blade angle β_c, Equation [15], presented in Fig. 8, and the solidity c/s, presented in Fig. 9. The solidity is given by the equation

$$c/s = \frac{2 \sin \beta_c \psi_e}{\eta C_L \phi_e} \quad \ldots\ldots\ldots\ldots\ldots\ldots [21]$$

where at the hub section, $\eta = \eta_1 = 0.6$. The reaction is sometimes of interest, and lines of constant reaction could be drawn in Fig. 6. The reaction is defined by

$$R = \frac{\dfrac{uV_{\theta\infty}}{g} - \dfrac{V_{\theta\infty}^2}{2g}}{\dfrac{uV_{\theta\infty}}{g}} = 1 - \frac{\psi_e}{2\eta^2} \quad \ldots\ldots\ldots\ldots [22]$$

It is important to consider that in general the efficiency is highest for high reactions and large C_L. This is in contrast to the conditions for least σ.

The suction specific speed is given by

$$N_{ss} = \frac{N_s}{\sigma^{3/4}} \quad \ldots\ldots\ldots\ldots\ldots\ldots [23]$$

and lines of constant N_{ss} are shown in Fig. 6. It should be noted that $N_{ss} = \text{const}$ is not an envelope line of the optimum-size lines although they are nearly equivalent at high values of specific speed.

In Fig. 10 the pressure-drop coefficient S has been plotted as a function of lift coefficient and per cent thickness to show the relative effects of these quantities. With regard to designing each radial section to have equal cavitation susceptibility, the exact requirement is that $S - 1/\sin^2 \beta_e$ be constant. It can be shown by example that this term does not vary more than 2 or 3 per cent from hub to case for normal cambers and thickness functions if the sections are designed with constant axial extent as previously proposed.

In making an impeller with optimum cavitation operation, it should be borne in mind that there is a large number of parameters involved and that certain choices must be made according to other requirements of the design. A minimum of curves has been presented with only the usual approach to a design considered. The basic equations have all been given to permit further calculation. In some instances other forms of the equations may be more appropriate.

DESIGN PROCEDURE

Generally for a new design, the head, flow rate, and desired submergence are given and certain motor speeds are available. From these quantities a trial specific speed can be computed. Choices of thickness and lift coefficient C_{L1} are made and a value of S is determined. Referring to charts, such as given in Fig. 6, will then show whether the computed σ can be achieved. If suitable choices will meet the requirements, then the corresponding hub blade angle β_e and c/s can be determined from Figs. 8 and 9. From the optimum value of $(\chi_{r_2})^4$ the fourth root can be used with Equation [18] to compute r_2. (The hub ratio η_1 is considered to have only the value 0.6 in this presentation.) Knowing r_2, c/s, and β_e, then a choice of number of blades n can be made and the chord c and axial extent z_t can be calculated. These quantities determine the basic blade design. If any of the foregoing quantities do not suit special requirements or turn out to be unreasonable (e.g., $c/s >> 1$ or β_e very small) then new choices must be made and the process repeated. The interference calculation was made for a hub blade angle of 32.4 deg. In Fig. 8, it is seen that the optimum blade angle is not too different from 30 deg for a wide range of specific speeds and values of C_L. Therefore the interference-calculation results should be reasonably appropriate for a large number of pump designs. In the event that the solidity is small, then the blade-to-blade interference may be neglected and the streamline can be calculated using a linear representation for the C_θ given in Equation [1] where the

[4] The camber shape is listed in reference (9) for 6 per cent camber as NACA 65. For other than 6 per cent camber the ordinates and lift coefficient are scaled linearly.

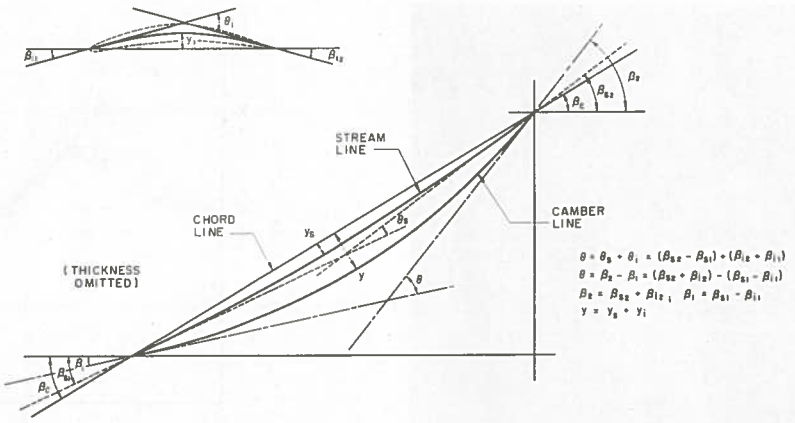

FIG. 11 GEOMETRY OF A BLADE SECTION

blade angle is not restricted. With the basic blade quantities chosen, the values of n and ξ_t are used to find values of K_0 and K_1 in Fig. 4, ψ_e and ϕ_e can be computed, and the streamline for several radial sections can be calculated from Equation [9]. (Note, the values of β_{c1} determined from Equations [4] and [15] should agree, although there may be an unimportant slight difference resulting from the use of plotted values.) The values of β_c and C_L at the other radial sections are computed from Equations [11] and [10].

The blade-section shapes may now be drawn. The simplest method is to plot the streamlines and then graphically place the camber on the streamline using NACA data scaled for the proper values of C_L. Thickness is added in the usual manner. A typical blade section is shown in Fig. 11. Some designers prefer using the camber angles instead of displacements, in which case the isolated camber angle may be added to the streamline "camber" angle and the resultant drawn from the straight chord line at the correct blade angle. The camber-angle method is also demonstrated in Fig. 11.

Mention has been made of the symmetrical parabolic camber lines (NACA 65) and the Series 16 thickness functions. The author believes that this combination gives an excellent pressure distribution for a pump impeller; however, other camber lines and thicknesses may be used with the design procedure.

EXPERIMENTAL STUDY

An experimental impeller was designed by the method presented and all of its descriptive quantities are given in Table 2. The angular and axial co-ordinates of the upper and lower blade surfaces were determined by spotting points and then trimming the material to these points. Plaster-mold halves were made and several identical blades were cast. The blades were bolted into a hub with the receiving slots machined at the correct angle. Sectional drawings of the vanes are shown in Fig. 12(*a*) and the test pump is shown in Fig. 12(*b*). No inlet or discharge vanes were employed as it was the purpose of this test to evaluate the impeller without any other influences.

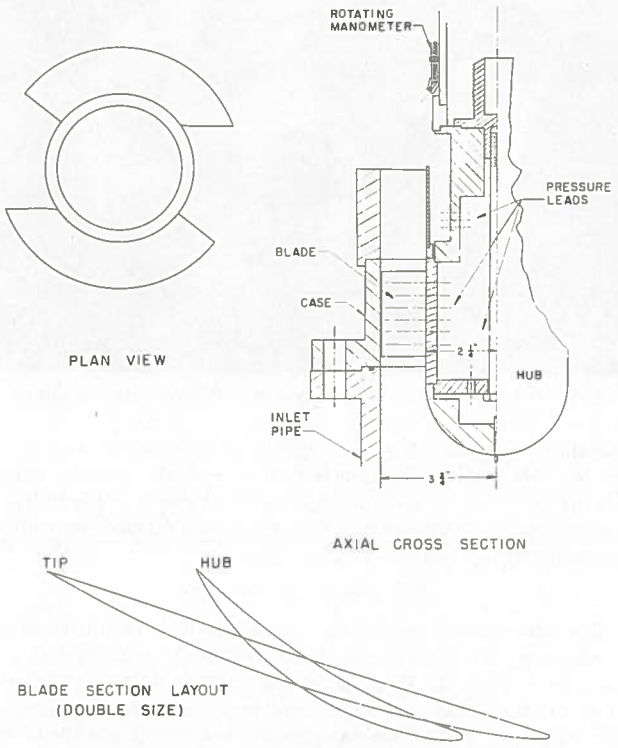

FIG. 12(*a*) VIEWS OF TEST PUMP AND BLADES

TABLE 2 VALUES DESCRIBING EXPERIMENTAL IMPELLER

Design performance coefficients $\psi_e = 0.126$, $\phi_e = 0.315$; expected $\phi_e = 0.295$

$r_1/r_2 = \eta_1 = 0.6$			$r_1 = 2.25$ in.			$r_2 = 3.75$ in.			
η	K_o	K_1	β_c, deg.	C_L	c, in.	c/s	β_1	β_2	θ
0.60	0.117	0.295	32.4	1.000	5.04	0.713	11.90	53.5	41.6
0.65	0.121	0.229	29.5	0.845	5.49	0.716	12.5	46.7	34.2
0.70	0.125	0.191	27.2	0.728	5.91	0.716	12.7	41.8	29.1
0.75	0.126	0.167	25.3	0.636	6.32	0.715	12.7	37.9	25.2
0.80	0.123	0.151	23.6	0.558	6.74	0.716	12.6	34.6	22.0
0.85	0.121	0.142	22.1	0.493	7.18	0.717	12.5	31.8	19.4
0.90	0.115	0.139	20.9	0.441	7.59	0.716	12.2	29.5	17.3
0.95	0.104	0.137	19.7	0.393	8.04	0.718	11.9	27.4	15.5
1.00	0.090	0.137	18.6	0.355	8.46	0.718	11.6	25.5	13.9

$\xi_t = 0.72$ $z_t = 2.7$ in. Test rpm = 210

For N = 210; Q (cfs) = 1.35 ϕ_e, H (ft) = 1.47 ψ (or C_p)

Calculated coefficients: $N_s = 10,300$, $\sigma' = 1.7$ $N_{ss} = 6,900$

C_L of isolated airfoil that is placed on curved streamline.

The experimental facilities and testing techniques of the rotating channels laboratory of the California Institute of Technology have been described many times in Hydrodynamics Laboratory reports. Briefly, the test impeller is driven by a dynamometer which permits torque measurement and is speed-controlled. The flow rate is measured with venturi meters. Impeller-head measurement is made with total-head probes at the impeller inlet and immediately behind the impeller blades. Static-pressure distributions on the blades were measured by casting static tap leads into the blades which connect with a manometer rotating with the

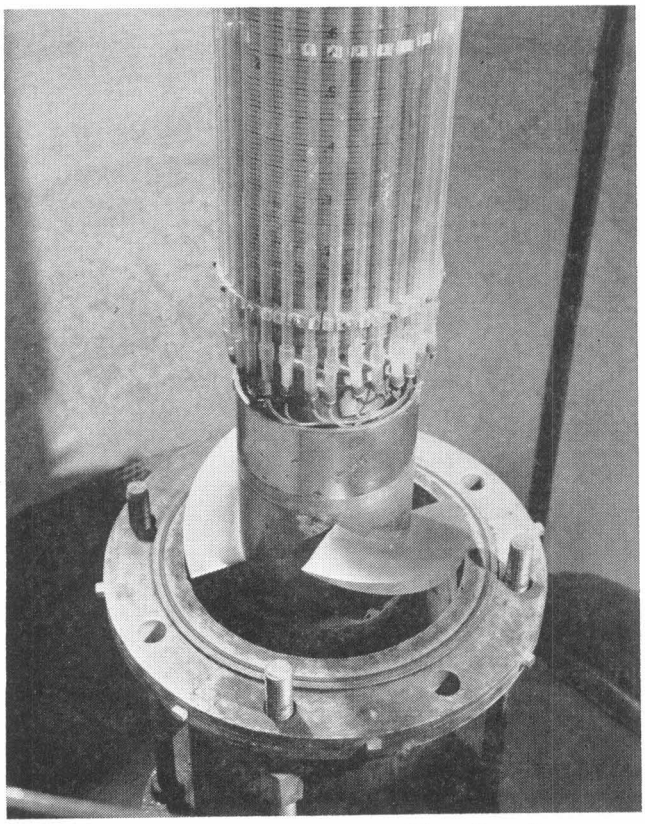

FIG. 12(b) INSTRUMENTED IMPELLER WITH CASE REMOVED

impeller. In addition to the impeller measurements, a velocity survey was made at the impeller inlet (with the impeller blades absent) in order to determine the real fluid effects of the hub and case on the model operation. The accuracy of all measurements is probably within two per cent.

EXPERIMENTAL RESULTS

The experimental results are reported in terms of dimensionless coefficients. In Fig. 13, the head coefficients measured at five radii are presented. The interesting result is that all radial sections produce nearly the same head over a considerable range of flow rate. When deviation begins, the hub, which has the heaviest loading, stalls off first. Then successive radial sections stall, the tip section being the last to stall. A weighted average of the five head curves was taken as the head of the impeller, and the *resultant* characteristic curves are shown in Fig. 14. The performance is compared with the predicted values by first considering the inlet-velocity profile shown in Fig. 15. There it is seen that the axial-velocity component is about 5 to 7 per cent above the average value over the greater portion of the passageway. Thus, in Fig. 14, the calculated value of design performance as indicated by the dotted cross is corrected by 6 per cent to give an expected design point indicated by the solid cross. It is seen that the head produced is about 4 per cent lower than the expected design point, whereas the "input" head ψ' is about 1 to 2 per cent greater. The input head is the head that would be produced if the efficiency were 100 per cent and is found by dividing the torque by the flow rate τ/ϕ. The input head is the one that should correspond to the theory. Thus it is seen that the expected design performance was closely achieved in the experimental test.

The best efficiency point occurs close to the expected design

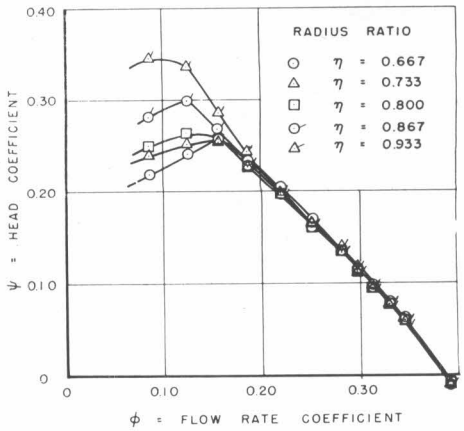

FIG. 13 DEVELOPED HEAD COEFFICIENT MEASURED AT FIVE RADIAL POSITIONS

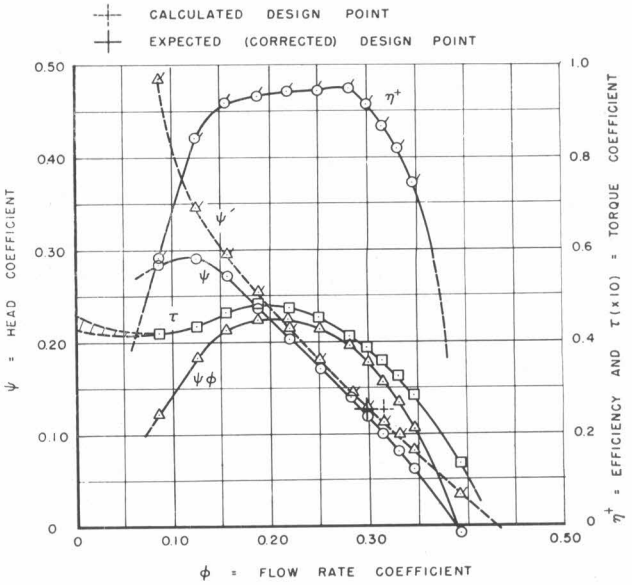

FIG. 14 PERFORMANCE CHARACTERISTICS OF TEST IMPELLER

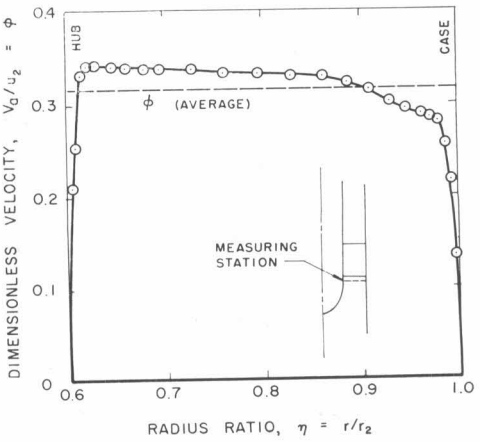

FIG. 15 MEASURED INLET-VELOCITY PROFILE

point; however, the shape of the efficiency curve is of special interest. The efficiency drops off rapidly beyond the maximum point, although at flow rates from one half the design value up to the design point the efficiency is high. The best efficiency point occurs at a flow rate about 4 per cent below design. Thus the design point is at the high flow-rate end of the high-efficiency range. This results from considering the design flow rate to be the "shockless" entry flow rate corresponding to zero angle of attack. Operating at small positive angles of attack evidently gives better efficiency. At negative angles of attack the operation is not good.

In Fig. 16 the static head (pressure) distribution on the blades of the pump is shown as a function of the flow rate for several radii. At flow rates below the expected design point it can be seen that there are large pressure differences at the leading edges of the blades corresponding to the positive angle of attack. Above the expected design flow rate the angle of attack is negative and the resultant pressure distributions are "crossed over." Near expected design flow rate the flow streams smoothly onto the blade giving an oval-shaped pressure profile. The actual shockless point seems to occur at a flow rate slightly greater than $\phi = 0.284$ which is about 4 per cent less than the expected design point. The correspondence of the correct pressure distribution and the best efficiency is excellent. The 4 per cent deviation

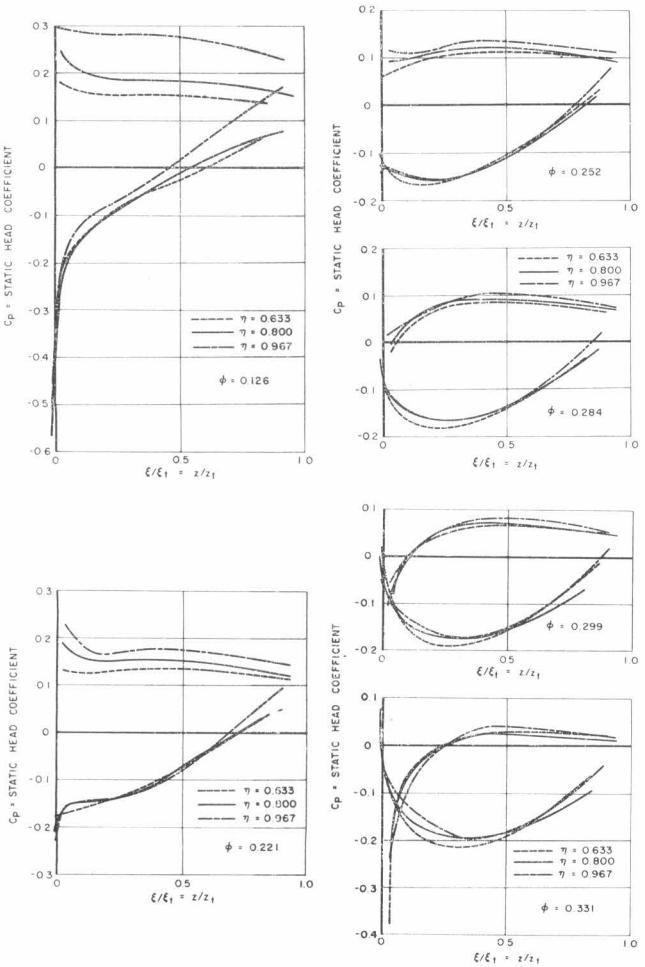

FIG. 16 STATIC HEAD DISTRIBUTION AS A FUNCTION OF AXIAL EXTENT

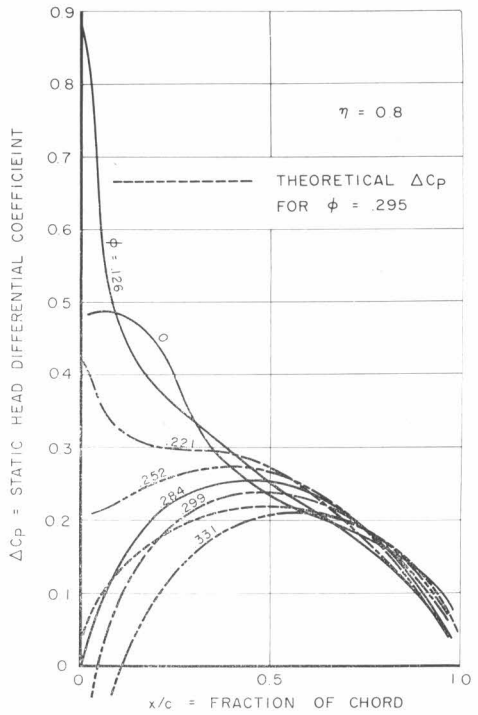

FIG. 17 STATIC HEAD DIFFERENTIALS AS A FUNCTION OF CHORD AT MID-RADIUS POSITION

from the expected design point represents the maximum error in the performance prediction. In Fig. 17 the pressure differentials along the blade have been plotted and the smooth entry point is again demonstrated. The theoretical pressure differential is plotted at the expected design flow rate and the agreement is favorable.

From the minimum value of static-head coefficient in Fig. 16, the experimental cavitation operation can be determined. For incipient cavitation, $(—)C_P$ is a dimensionless NPSH and $\sigma = (—)C_P/\psi$. Both $(—)C_P$ and σ are plotted in Fig. 18 and the value of σ determined by the optimizing analysis is indicated. It is seen that operation at small angle of attack is not detrimental to cavitation susceptibility, but the true best *cavitation coefficient* does occur at the shockless entry flow rate. It is of interest to note that σ is less at a lower flow rate than $(—)C_P$ due to the greater increase of ψ. However, σ plotted as a function of flow rate is misleading; NPSH is the absolute quantity to consider.

DISCUSSION

The agreement between the theoretical performance predicted by the design procedure and the performance achieved is believed to be good. The best efficiency point, the shockless entry point, and best conditions for cavitation all occur at the same flow rate, which is about 4 per cent less than the expected design point. The design method predictions and the experimental results agree then to within 5 per cent. This discrepancy is not large and may be due to any number of causes. In Fig. 19 a comparison of the experimental performance (based on C_L), the performance predicted by the design procedure, and the performance of the blade shape as an isolated airfoil is made as percentage of the isolated performance. Also shown are the results of two modern cascade theories. The usefulness of the present design method is clearly demonstrated.

One result of the experimental work that was not expected

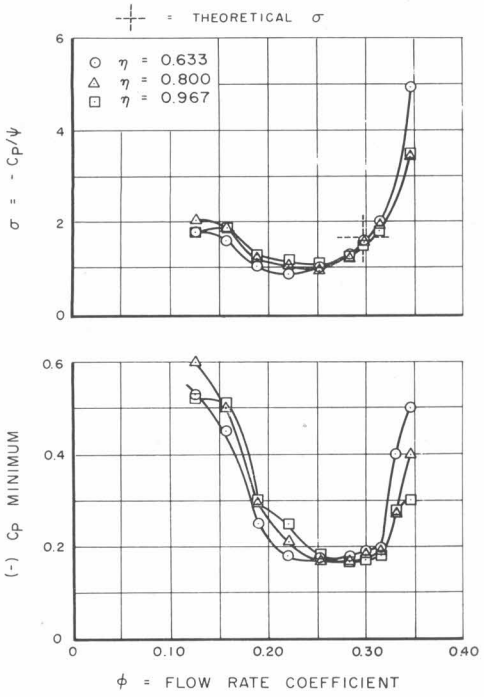

FIG. 18 INCIPIENT CAVITATION COEFFICIENT DETERMINED FROM STATIC HEAD DISTRIBUTION

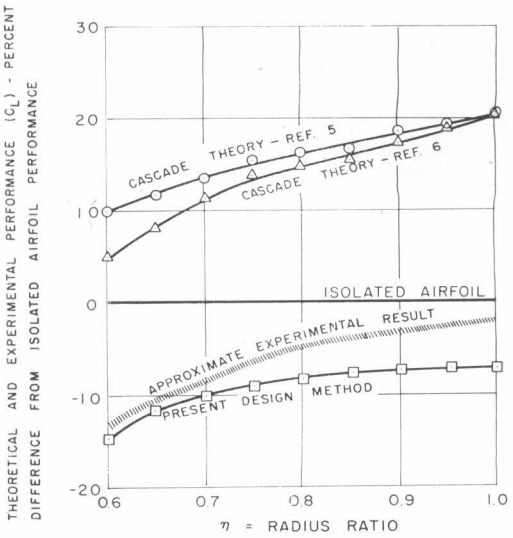

FIG. 19 COMPARISON OF THEORETICAL EXPECTATION AND EXPERIMENTAL RESULT AS PERCENTAGE FROM ISOLATED AIRFOIL PERFORMANCE

concerns the nearly similar head developed at all radial sections over a large range of flow rate. This means that free-vortex operation is approximate over a range of flow rather than at a single flow rate, as is the usual case. This result is not completely understood at the present time. The design method was only intended to deal with the desired design performance quantities, so investigation of the prediction of off-design performance would provide valuable additional material for the present procedure.

With regard to the allowance for the inlet-velocity profile in evaluating the experimental results, it is important to realize that the inlet of the test setup consisted of a long section of pipe which permitted growth of a thick boundary layer. The inlet of a normal commercial pump should not include this boundary-layer difficulty and no allowances in the design procedure would be necessary.

For the complete pump a diffusing section also must be considered. The experimental impeller herein described has a reaction of from 90 to 95 per cent at the design point. This means that only about 5 to 10 per cent of the total energy produced by the impeller is recoverable from the tangential-velocity component. It seems reasonable then that diffusing blades need not be very large or heavily loaded. In fact considering that diffusion blades in themselves will add losses, perhaps the most efficient diffuser in this case would be no diffuser blades at all. In cases where the reaction is lower and diffuser blades are necessary, then from interference consideration the diffuser blades should be some distance removed downstream of the impeller. If the diffuser-blade row is quite close to the impeller, proper prediction of impeller performance cannot be made. More complete investigation of diffuser influence on impeller operation is another desirable addition for this design procedure.

ACKNOWLEDGMENT

Acknowledgment is made to Profs. D. A. Morelli and A. J. Acosta for their interest and very helpful advice.

BIBLIOGRAPHY

1 "Pressure Distributions on the Blade of an Axial-Flow Propeller Pump," by D. A. Morelli and R. D. Bowerman, Trans. ASME, vol. 75, 1953, pp. 1007–1013.

2 "Three-Dimensional Interference Effects of a Finite Number of Blades in an Axial Turbomachine," by H. N. Tyson, Jr., Hydrodynamics Laboratory Report E-19.1, California Institute of Technology, November, 1952.

3 "The Design of Propeller Pumps and Fans," by M. P. O'Brien and R. G. Folsom, University of California Publications in Engineering, vol. 4, no. 1, 1939.

4 "Analysis of Modern Propeller-Pump Design," by W. Spannhake, David W. Taylor Model Basin Report 621, June, 1948.

5 "Theoretical and Experimental Investigations of Axial Flow Compressors," by J. T. Bowen, R. H. Sabersky, and W. D. Rannie, report on research conducted under contract with the Office of Naval Research, California Institute of Technology, Pasadena, Calif., 1949.

6 "An Approximate Theory for Potential Flow Through Cascades of Airfoils," by G. E. Hlavka, PhD thesis, California Institute of Technology, Pasadena, Calif., 1954.

7 "Fluid Mechanics of Turbomachinery," by G. F. Wislicenus, McGraw-Hill Book Company, Inc., New York, N. Y., 1947.

8 "Problems and Results of Investigations on Cascade Flow," by H. Schlichting, *Journal of the Aeronautical Sciences*, vol. 21, no. 3, 1954, p. 163.

9 "Summary of Airfoil Data," by I. H. Abbott, A. E. von Doenhoff, and L. S. Stivers, Jr., NACA TR 824, 1945.

10 "Principles of Rocket-Turbopump Design," by C. C. Ross, *American Rocket Society Journal*, vol. 21, March, 1951, pp. 21–33.